

Cite this: DOI: 00.0000/xxxxxxxxxx

Received Date  
Accepted Date

DOI: 00.0000/xxxxxxxxxx

Exploring the Influence of  $(n-1)d$  Subvalence Correlation and of Spin-Orbit Coupling on Chalcogen Bonding<sup>†</sup>Nisha Mehta<sup>\*a‡</sup> and Jan M. L. Martin<sup>b</sup>

This article presents a comprehensive computational investigation into chalcogen bonding interactions, focusing specifically on elucidating the role of subvalence  $(n-1)d$  and  $(n-1)sp$  correlation. The incorporation of inner-shell  $(n-1)d$  correlation leads to a decrease in interaction energies for chalcogen-bonded systems (at least those studied herein), contradicting the observations regarding halogen bonding documented by Kesharwani et al. in *J. Phys. Chem. A*, **2018**, 122 (8), 2184-2197. The significance of  $(n-1)sp$  subvalence correlation appears to be lower by an order of magnitude. Notably, among the various components of interaction energies computed at the PNO-LCCSD(T) or DF-CCSD levels, we identify the PNO-LMP2 or DF-MP2 component of the  $(n-1)d$  correlation as predominant. Furthermore, we delve into the impact of second-order spin-orbit coupling (SOC2) on these interactions. Specifically, for the Te complexes, SOC2 effects rival  $(n-1)d$  correlation in importance; for the Se complexes, SOC2 is much less important. Generally, SOC2 stabilizes monomers more than dimers, resulting in reduced binding of the latter. Notably, at equilibrium and stretched geometries, SOC2 and  $(n-1)d$  destabilize the complex; however, at compressed geometries, they exhibit opposing effects, with  $(n-1)d$  becoming stabilizing.

## 1 Introduction

Non-covalent interactions exert a crucial influence on the physical and chemical properties of diverse systems.<sup>1,2</sup> They are pivotal in processes such as protein folding, ligand interactions, packing and stacking arrangements, organocatalysis, supramolecular chemistry, and conformational stability, underscoring their significance across a spectrum of scientific disciplines.<sup>3,4</sup> A molecule featuring a chalcogen atom, such as sulfur, selenium, or tellurium, can partake in a multitude of non-covalent interactions, exemplified by phenomena such as chalcogen bonding, electrostatic interactions, and hydrogen bonding. Chalcogen bonding is a type of non-covalent interaction that involves the interactions between a chalcogen atom (chiefly S, Se, or Te) and a Lewis base or electron-rich region in the neighboring molecule. In a chalcogen bonding, a chalcogen atom functions as an electrophile, while the interacting partner contributes electron density to facilitate the interac-

tion. These interactions exhibit a pronounced directional character. The importance of chalcogen bonding interactions lies in their role as a unique and versatile class of noncovalent interactions, influencing molecular recognition, supramolecular assembly, and crystal engineering, with potential applications in drug design, materials science, and catalysis.<sup>5-17</sup>

Numerous systems engage in chalcogen bonding via the  $\sigma$ -hole; nonetheless, an alternative avenue involves the  $\pi$ -hole. This distinctive  $\pi$ -hole constitutes a positively charged domain, positioned orthogonally to a planar  $\pi$ -framework. This positive region demonstrates an affinity for interacting with electron donors. Illustrative instances encompass interactions like  $\text{SO}_3 \cdots \text{H}_2\text{O}$ ,<sup>18-20</sup>  $\text{SO}_3 \cdots \text{NH}_3$ ,<sup>21-23</sup>  $(\text{SO}_3)_n \cdots \text{H}_2\text{CO}$ ,<sup>24,25</sup>  $(\text{SO}_3)_n \cdots \text{CO}$ ,<sup>26</sup> and  $(\text{SO}_3)_n \cdots (\text{CO})_n$ ,<sup>26</sup> where  $n=1,2$ .

Computational methodologies, such as *ab-initio* calculations, play a pivotal role in the examination of chalcogen bonding interactions. It enables precise predictions of molecular structures, energetics, and electronic properties, yielding invaluable insights that might pose challenges or prove unattainable through experimental means. Furthermore, the results can function as a reference point for refining less expensive computational approaches, like DFT and force field methods. Nonetheless, to conduct a thorough benchmark study, it is imperative to accumulate statistics from a sufficiently extensive array of calculations. Illustrative examples of such comprehensive datasets include the  $G_n$  test

<sup>a</sup> Department of Molecular Chemistry and Materials Science, Weizmann Institute of Science, 7610001 Rehovot, Israel; E-mail: nisha.mehta@weizmann.ac.il.

<sup>b</sup> Department of Molecular Chemistry and Materials Science, Weizmann Institute of Science, 7610001 Rehovot, Israel.

<sup>†</sup> Electronic Supplementary Information (ESI) available: Spreadsheet containing RMSD at various levels of theory, results of SAPT and other NCI indices; Cartesian coordinates (in .xyz format) of 24 structures; Interaction energies at various levels of theory (in .txt format); See DOI: 10.1039/cXCP00000x/

<sup>‡</sup> Present address: School of Chemistry, The University of Melbourne, VIC 3010, Australia.

sets,<sup>27–30</sup> database 2015B,<sup>31</sup> MGCD84 (Main Group Chemistry Data Base, 84 subsets) of the Berkeley group,<sup>32</sup> and the Grimme and Goerigk groups' GMTKN55<sup>33</sup> dataset (general main-group thermochemistry, kinetics, and noncovalent interactions, 55 problem sets), as well as the latter's predecessors GMTKN24<sup>34</sup> and GMTKN30.<sup>35</sup> These extensive databases encompass a diverse array of benchmark sets, including directional non-covalent interactions such as hydrogen and halogen bonding. While prior research extensively explored halogen bonding interactions, as detailed in the references, it is noteworthy that the aforementioned datasets do not encompass complexes representing chalcogen bonding interactions. To address this gap, one of us and coworkers previously developed the CHAL336 benchmark<sup>36</sup> comprising 336 chalcogen-bonded dimers, hitherto the largest and most accurate of its kind.

As we delve into the intricacies of chalcogen bonding, our focus narrows down to a crucial and often overlooked aspect—the importance of subvalence  $(n-1)d$  and  $(n-1)sp$  correlation contributions to chalcogen bonding interactions. For other types of noncovalent interactions, especially involving lighter elements, inner-shell correlation is routinely neglected — this is easy to justify for elements like O and even S, where the core-valence gaps are 19.43 and 5.81 Hartree, respectively. For Se and Te, however, the outer-core  $(n-1)d$  orbitals lie just 1.8 and 1.3 Hartree, respectively, below the valence shell — even smaller than in the adjacent halogens Br and I, for which it has previously been shown<sup>37</sup> that  $(n-1)d$  correlation contributes quite significantly to the interaction energy, particularly at shorter distances.

However, if we include core-valence effects, it behooves us to also consider whether other contributions could not be of similar importance. What comes to mind in particular is spin-orbit coupling (SOC), a quantum phenomenon resulting from the interaction between an electron's spin and the magnetic field generated by its orbital motion around the nucleus. SOC can exert a significant influence on the electronic and magnetic properties of materials, particularly those containing heavy elements with large atomic numbers. Closed-shell systems are not subject to first-order SOC, but they may be stabilized by second-order SOC (SOC2: see, e.g.,<sup>38–41</sup>). For instance, De Jong and coworkers<sup>42</sup> found for HBr, Br<sub>2</sub>, HI, and I<sub>2</sub> 2nd order SOC stabilizations of {0.1, 0.4, 0.5, 2.0} kcal/mol, respectively. An experimental manifestation of SOC2 is the zero-field splitting (ZFS) in the  $X^3\Sigma^-$  ground states of chalcogen diatomics: see, e.g., Table 6 in Ref.<sup>43</sup>, where one finds ZFS of 23.5 cm<sup>-1</sup> for S<sub>2</sub>, 510 cm<sup>-1</sup> for Se<sub>2</sub>, and 1975 cm<sup>-1</sup> for Te<sub>2</sub>. (That is, 0.067, 1.458, and 5.647 kcal/mol, respectively — note a rough  $Z^4$  dependence on the atomic number  $Z$  as conjectured in Ref.<sup>44</sup> and noted, in a solid state physics context, in Ref.<sup>45</sup>.) As such numbers are actually in the same energetic range as the subvalence (outer-core) correlation effects we are considering here, we ought to at least attempt to gauge the importance of SOC2 for chalcogen bonding interactions, and compare its importance with that of outer-core correlation.

## 2 Computational details

We have selected TeO<sub>3</sub>⋯TeHF, SeO<sub>3</sub>⋯SeHF, and SO<sub>3</sub>⋯SHF as exemplars of chalcogen bonding interactions involving Te, Se,

and S, respectively. In this study, the reference geometries for TeO<sub>3</sub>⋯TeHF, SeO<sub>3</sub>⋯SeHF, and SO<sub>3</sub>⋯SHF were acquired from Ref. 36 and employed without additional optimization. The original 1.0 $r_e$  structure had undergone optimization using the PW6B95-D3(BJ) method with a def2-TZVPD basis set. In our current study, we determined the remaining structures through stretching and compressing the intermonomer distance (with frozen monomer geometries) by scaling factors of {0.80, 0.85, 0.90, 0.95, 1.0, 1.05, 1.10, 1.25, 1.50, 2.0} using an in-house Python script. The XYZ coordinates for all 30 structures can be found in the Supporting Information. Initially, we included compressed distances of 0.80 $r_e$  and 0.85 $r_e$ ; however, we subsequently opted to omit them due to the strong intermonomer repulsion at such compressed geometries. Consequently, the statistics presented in this manuscript pertain to distances of {0.90, 0.95, 1.0, 1.05, 1.10, 1.25, 1.50, 2.0}, totaling 24 dimers.

The computations were conducted on the "ChemFarm" HPC cluster of the Faculty of Chemistry at the Weizmann Institute of Science. All *ab initio* calculations, both canonical and localized, were performed using MOLPRO 2023.2<sup>46</sup>. Specifically, we employed a combination of Dunning correlation-consistent cc-pVnZ (where  $n = D, T, Q, 5$ ) basis sets<sup>47</sup> for hydrogen atoms, along with their corresponding augmented counterparts, aug-cc-pVnZ,<sup>48</sup> for non-hydrogen atoms other than the chalcogens sulfur, for which we employed aug-cc-pwCVnZ,<sup>49,50</sup> and selenium and tellurium, for which we utilized aug-cc-pwCVnZ-PP<sup>51–53</sup>. (In this context, we would like to mention Ref. 54 and references therein, which recommended the incorporation of aug-cc-pwCVnZ basis sets for the accurate treatment of core-electron correlation.)

Our canonical calculations were limited to the density fitting CCSD (coupled cluster with iterative singles and doubles<sup>55</sup>) level as implemented in MOLPRO. For the higher CCSD(T) level,<sup>56</sup> we employed localized orbital CCSD(T) approximations, and specifically the PNO-LCCSD(T) method (pair natural orbital localized coupled cluster, see Ref.<sup>57</sup> for a review), and using the DomOpt=Normal, Tight, and vTight threshold combination as detailed in the MOLPRO 2024 online manual<sup>58</sup> — which for Tight differ slightly from the original values given in Ma and Werner.<sup>59</sup>

Basis set extrapolation was carried out by means of the two-point extrapolation formula  $E_L = E_\infty + B/L^\alpha$ , where  $L$  denotes the maximum angular momentum present within the basis set and  $\alpha$  represents the exponent associated with the level of theory and basis set pair. Equivalently, this can be written in the Schwenke<sup>61</sup> form  $E_\infty = E_L + A_L(E_L - E_{L-1})$ , if the Schwenke extrapolation coefficient  $A_L = ((\frac{L}{L-1})^\alpha - 1)^{-1}$ . (For a discussion of the equivalence relations between the various two-point extrapolation formulas, see Ref.<sup>60</sup>.)

For the HF, MP2, CCSD, and (T), our {T,Q}Z Schwenke coefficients are 0.415, 0.915, 0.700, and 0.730, respectively, taken from Refs.<sup>60,62</sup> Likewise, for the {Q,5}Z extrapolation, the corresponding values are 0.528, 1.186, 0.930, and 0.810. It should be noted that we employed identical extrapolation exponents for both the localized and canonical methods, as they should converge to the same result.

Spin-orbit coupling calculations were performed using the

Time-Dependent Density Functional Theory (TD-DFT) module implemented in the ORCA software package (version 5.0.2).<sup>63–65</sup> The Zeroth Order Regular Approximation (ZORA) method was employed to account for scalar relativistic effects.<sup>66</sup> The CAM-B3LYP range-separated hybrid<sup>67</sup> with the aug-cc-pVQZ-DK basis set<sup>49,50,68,69</sup> was employed. Among the auxiliary basis sets SARC/J,<sup>70–74</sup> and def2-QZVPP/C<sup>75,76</sup> were employed. Spin-orbit integrals were evaluated within the RI-SOMF(1X) approximation<sup>77</sup>.

In addition to the Boys-Bernardi counterpoise corrections<sup>78</sup> and the original "raw" (uncorrected) values, we also employ the mean of both (referred to as "half-CP"), a practice rationalized by Sherrill et al.<sup>79</sup> and by Brauer et al.<sup>80</sup>.

Finally, symmetry-adapted perturbation theory (SAPT, see Ref.<sup>81</sup> for a review) calculations were performed employing the SAPT module<sup>82</sup> within the PSI4 software framework<sup>83</sup>.

### 3 Results and discussion

The complete list of the 24 chalcogen-bonded systems, together with our best values for the interaction energies obtained in the present work, is outlined in the final two columns of Table 4. Due to hardware limitations, we were unable to compute interaction energies utilizing the haWCV5Z basis set at the canonical CCSD level, nor could we incorporate (T). Therefore, our canonical calculations were limited to the DF-CCSD/haWCV{T,Q}Z level. However, we were able to conduct computations using the 5Z-sized basis set through the localized PNO-LCCSD(T) scheme. We have selected the composite PNO-LCCSD(T) approach, opting for the Tight/{Q,5}Z+0.5[vTight-Tight]/{T,Q}Z half-CP as our optimal reference level. In the subsequent sections of this manuscript, we referred to this scheme as cPNO-LCCSD(T). Although we will delve into this more thoroughly in the following section, it is crucial to note that our reference level (i.e., PNO-LCCSD(T) Tight/{Q,5}Z+0.5[vTight-Tight]/{T,Q}Z half-CP) exhibits an RMSD of just 0.054 kcal/mol when compared to both the raw and full-CP counterparts (Table 1). Needless to say, at the true CBS limit, the difference between raw and CP-corrected values should be zero: a significant discrepancy between raw and CP in a CBS extrapolation suggests that the underlying calculations are inadequate or that the extrapolation procedure is problematic or both.

We performed three distinct sets of computations: (i) solely considering valence electrons, (ii) including valence and (n–1)d electrons, and (iii) encompassing valence, (n–1)d, and (n–1)sp electrons. Unless otherwise specified, the statistical analyses presented in subsequent section pertains to 'valence + (n–1)d electrons'.

#### 3.1 Some observations on the counterpoise corrections for the chalcogen bonding interactions

First we wish to establish how basis set superposition error (BSSE) behaves for different components of the interaction energy (SCF, MP2 correlation, and post-MP2 correction) and obtain interaction energies with basis sets large enough that BSSE has been reduced to insignificance. It has been argued numerous time

in the literature (perhaps the first time by Helgaker and coworkers<sup>84</sup>) that  $BE_{raw}$  and  $BE_{CP}$  tend to converge to the CBS limit from opposite directions: hence,  $BE_{half-CP} = (BE_{raw} + BE_{half-CP})/2$  naturally suggests itself as the optimal choice (see Refs. 79,80 and references therein). When observing smaller RMSDs for CP-uncorrected results, this is mainly due to error compensation between BSSE (which causes overbinding) and intrinsic basis set insufficiency (IBSI, which leads to underbinding).<sup>80</sup> In such cases, this suggests the need for larger basis sets. It has been shown in the past (e.g., Ref.<sup>62,79</sup>) that even a 5Z-sized basis set may still be too far from CBS for an MP2 or coupled cluster calculation for its BSSE to outweigh its IBSE; hence, applying half-CP correction on top of {Q,5}Z extrapolation appears to be more appropriate.

#### SCF and MP2 components

First, let us delve into the HF level. In our computations using HF/haWCV{Q,5}Z, the impact of counterpoise corrections appears minor, albeit non-negligible: the root mean square deviation (RMSD) between half-CP versus full-CP and raw data stands at 0.010 kcal/mol. Examination of Table 1 demonstrates that at haWCV5Z and haWCVQZ levels, all three variants—raw, half-CP, and full-CP—result in approximately 3-fold and 8-fold increases in RMSD values, respectively. Furthermore, the {T,Q}Z half-CP demonstrates a considerable 0.225 kcal/mol RMSD disparity from the reference value, which is quite substantial. At the TZ level, the RMSD becomes more pronounced, reaching 0.393 kcal/mol for the half-CP.

Thus, we observed a slower-than-usual convergence of basis sets for the SCF component. Although no systematic trend is evident, Table 1 suggests that basis set convergence is slower for sulfur-based complexes, followed by tellurium and selenium.

Let us next consider the MP2 correlation component. At the composite cPNO-LMP2 level (i.e., PNO-LMP2/[Tight/{Q,5}Z+0.5[vTight-Tight]/{T,Q}Z]), the RMSD of half-CP with both CP-corrected and uncorrected interaction energies is just 0.023 kcal/mol. For PNO-LMP2/aWCV{Q,5}Z level, half-CP clearly agrees best with the composite cPNO-LMP2 half-CP reference level (RMSDs are 0.025, 0.003 and 0.023 kcal/mol, respectively for raw, half-CP and full-CP).

In fact, {T,Q}Z extrapolation seems to yield lower RMSDs than 5Z. As an example, 5Z yields RMSD of 0.498 kcal/mol, in comparison to just 0.073 kcal/mol for {T,Q}Z, this is even the case for post-MP2 corrections as well, which we will be discussing next. It appears that {T,Q}Z extrapolation may potentially yields superior results compared to utilizing the 6Z basis set. For example, in a very recent study on basis set extrapolations,<sup>85</sup> it has been shown that for the W4-17 thermochemical benchmark<sup>86</sup>, the RMSD computed for BSSEs at the CCSD/haVnZ+d level are {3.94, 1.74, 0.77, 0.31} kcal/mol for  $n = \{T, Q, 5, 6\}$ , in contrast to 0.27 kcal/mol for haV{T,Q}Z and 0.13 kcal/mol for haV{Q,5}Z.

We observed a significant increase in RMSDs upon incorporating Counterpoise (CP) correction. Sorting by RMSD may suggest that opting for the "raw" data is optimal for the majority of basis sets. For instance, even for a 5Z-sized basis set, the RMSD increases from 0.328 kcal/mol to 0.498 and 0.669 kcal/mol upon incorporating half and full CP corrections, respectively. However,

this does not imply that one should avoid using counterpoise correction. Rather, as explained at length by Sherrill and coworkers<sup>79</sup> for orbital-based calculations, and by Brauer et al.<sup>80</sup> for explicitly correlated ones, such ‘right trends for the wrong reason’ reflect that ‘counterpoise-uncorrected’ interaction energies suffer from error compensation between BSSE and IBSI. In such cases, larger basis sets are indicated.

Furthermore, canonical DF-MP2 calculations using the haWCV{T,Q}Z extrapolation with half-counterpoise correction yield an RMSD of only 0.059 kcal/mol from the localized reference level. This suggests that both our localized and canonical outcomes are converging towards the same basis set limit, affirming that any observations made with the localized scheme are not merely artifacts of its usage.

### Post MP2 correction

Next, let us delve into the post-MP2 correlation components. Beginning with the CCSD-MP2 differences, at the reference level (cPNO-LCCSD–cPNO-LMP2), the difference between half-CP values and CP-corrected and uncorrected interaction energies is merely 0.028 kcal/mol RMSD.

It is noteworthy that the CCSD-MP2 term exhibits a more rapid basis set convergence compared to the MP2 term discussed earlier (refer to Table 1). Interestingly, this finding contradicts the trend observed for atomization energies, as documented by Ranasinghe and Petersson.<sup>87</sup>

At the haWCV{Q,5}Z level with half-CP and a tight threshold, the RMSD is merely 0.012 kcal/mol, which is lower than for full-CP and raw results. Furthermore, at the {T,Q}Z/Tight level, the RMSD for half-CP is just 0.046 kcal/mol, slightly lower than for full-CP (0.043 kcal/mol) but lower than for uncorrected results (0.077 kcal/mol). RMSD values at the canonical DF-CCSD–DF-MP2/haWCV{T,Q}Z are equally small (0.120, 0.076 and 0.044 kcal/mol, respectively, for the full-CP, half-CP and ‘raw’ results).

What about the CCSD(T)–MP2 component? At the reference level (cPNO-LCCSD(T)–cPNO-LMP2), the discrepancy between half-CP values and CP-corrected and uncorrected interaction energies is merely 0.029 kcal/mol RMSD—comparable in magnitude to what we observed for the CCSD–MP2 component. While it is customary in noncovalent interactions to generally consider CCSD(T)–MP2 together without further separation, in this study, it may be worthwhile to delve into the (T) component separately. This is particularly relevant for the upcoming section, where we will explore that the incorporation of subvalence (n–1)d electrons—central to the focus of this manuscript—may not significantly impact the (T) component. It’s worth noting that the basis set convergence of the (T) component is faster compared to MP2 and CCSD–MP2 components. Uncorrected and counterpoise-corrected composite-(T)/haWCV{Q,5}Z results are practically identical, with an RMS difference of only 0.006 kcal/mol. Both (T)/{T,Q}Z and {Q,5}Z extrapolation with tight settings and half-CP yield RMSDs of 0.047 and 0.033 kcal/mol, respectively. Once more, for most basis sets without CBS extrapolation, counterpoise corrections seem to be disadvantageous.

In summary, for chalcogen bonding interactions, CP correction generally worsens the statistical outcomes even with basis sets

as large as 5Z—owing to error cancellation between basis set superposition error and intrinsic basis set insufficiency, highlighting the necessity of employing large basis sets, particularly for the MP2 component, when studying such interactions. It seems that employing CBS extrapolation and applying CP correction atop it represents the best strategy. Surprisingly, {T,Q}Z extrapolation surpasses the performance of the 5Z basis set.

### 3.2 Effect of (n–1)d and (n–1)sp subvalence electron correlation

To examine core-valence correlation contributions, we conducted three sets of calculations for a given level of theory: (i) valence electrons only, (ii) valence + (n–1)d electrons, and (iii) valence + (n–1)d + (n–1)sp electrons. The interaction energy contributions calculated are provided in Table 3 and SI.

At the cPNO-LCCSD(T) level, the (n–1)d inner-shell correlation component amounts to 0.893 and 0.428 kcal/mol RMS, respectively, for Te and Se complexes—a notably significant contribution. Similarly, calculations at the DF-CCSD/haWCV{T,Q}Z level indicate the importance of (n–1)d correlation components to be in the same range (0.866 and 0.424 kcal/mol, respectively for Te and Se).

Moreover, the incorporation of (n–1)sp correlation effects in Te-complexes marginally raises this difference by an RMSD of 0.067 kcal/mol at the cPNO-LCCSD(T) level. In the case of Se complexes, the RMSD is slightly higher at 0.191 kcal/mol, yet it remains an order of magnitude lower compared to what has been observed for (n–1)d subvalence correlation. The canonical calculation results are consistent with this: for instance, the respective values at the DF-CCSD/haWCV{T,Q}Z level are 0.043 and 0.186 kcal/mol for Te and Se complexes, respectively. These values clearly indicate that, while (n–1)d correlation contributions can indeed be nontrivial for the calculated interaction energies in the Te- and Se-containing species, the (n–1)sp contributions are of a lower order of magnitude and may thus be neglected.

Before we delve into more detail on the nature of incorporating (n–1)d inner shell correlation, we first should explore its basis set convergence, as shown in Table 2. A similar table for (n–1)sp is provided in the Supporting Information. Te complexes exhibit significantly slower basis set convergence for the (n–1)d inner shell correlation component compared to Se complexes. While exploring how BSSE behaves for the different components of the (n–1)d contribution to the total interaction energy (MP2 and post MP2-correction), we again noticed that for all tripleZ-5Z basis sets, CP correction mostly deteriorates the statistics. However, for CBS extrapolated values (where the lion’s share of basis set errors is already taken care of), CP correction does help. Once again, CP-uncorrected data benefits from error cancellation between BSSE and BSIE as their effects are in opposite directions. Furthermore, the (T) component of the (n–1)d correlation displays the most rapid basis set convergence.

Table 3 presents the (n–1)d component of the total interaction energies calculated at the localized cPNO-LCCSD(T) and canonical DF-CCSD/haWCV{T,Q}Z levels for all 24 systems studied herein. (The corresponding table for (n–1)sp can be found

in the Supporting Information). Among different components of cPNO-LCCSD(T) (or DF-CCSD), PNO-LMP2 (or DF-MP2) contributes the lion's share. The RMSD between valence and valence+subvalence (n-1)d for PNO-LMP2 is 1.134 kcal/mol. This discrepancy is not an artifact of the localized scheme, as we also obtained an RMSD of 1.154 kcal/mol at the MP2/haWCV{T,Q}Z level. The CCSD-MP2 component displays around one-fourth of the RMSD observed for MP2. Furthermore, the (T) component of the (n-1)d correlation is extremely small, measuring only 0.040 kcal/mol. These findings are crucial, as they might prove useful in future work. Keeping the calculations including (n-1)d correlation down to the MP2 level leads to substantial savings in CPU time and memory/mass storage overhead.

The (n-1)d correlation effects are smaller for Se than for Te (refer to Table 3 for details).

Furthermore, somewhat surprisingly, (n-1)d effects are repulsive for equilibrium and stretched geometries. As expected, these effects are gradually reduced for stretched geometries and effectively dwindle to very small values at  $2.0r_e$ . However, for compressed geometries, (n-1)d correlation effects are attractive for Te-complexes and around.

Conducting a similar examination on the (n-1)sp subvalence correlation reveals that in the case of Te-complexes, the (n-1)sp component of (T) is significantly larger than what was observed for (n-1)d (0.109 versus 0.040 kcal/mol), and consistently exhibits a repulsive nature.

Therefore, although the (n-1)sp subvalence component appears to be an order of magnitude smaller than the (n-1)d contribution in the total cPNO-LCCSD(T) energies, the PNO-LMP2 and (T) corrections operate in opposite directions, resulting in error cancellation at the cPNO-LCCSD(T) level. Thus, it is imperative to incorporate (n-1)sp subvalence correction as well, particularly when our calculations are confined to the MP2 level.

### 3.3 Spin-orbit coupling

The above observations concerning the importance of subvalence correlation might lead the reader to wonder whether, for such heavy elements as Te, second-order spin-orbit coupling (SOC2) might not be of comparable importance. (As all species considered here are closed-shell singlets, there is no first-order spin-orbit contribution.) We computed SOC2 for each of the 24 chalcogen-bonded dimers using the SOC-TD-DFT code in ORCA, at the all-electron CAM-B3LYP/aug-cc-pVQZ-DK level.

Figure 1 illustrates the SOC2-induced stabilization of the ground state in relation to the binding energies of all 24 systems at the CAM-B3LYP/aug-cc-pVQZ-DK level. Additionally, the plot depicts the magnitude of inner-shell subvalence (n-1)d and (n-1)sp correlation contributions, as discussed in the preceding section, at the cPNO-LCCSD(T) level.

For  $\text{TeO}_3 \cdots \text{TeHF}$  complexes, at equilibrium separation, both SOC2 and the inner-shell subvalence (n-1)d contribute to the destabilization of the dimer. However, the effect of SOC2 is more significant at  $-2.119$  kcal/mol, compared to the (n-1)d contribution which is only  $-0.386$  kcal/mol. Upon compression of the dimer, SOC2 continues to contribute approximately  $-2$  kcal/mol

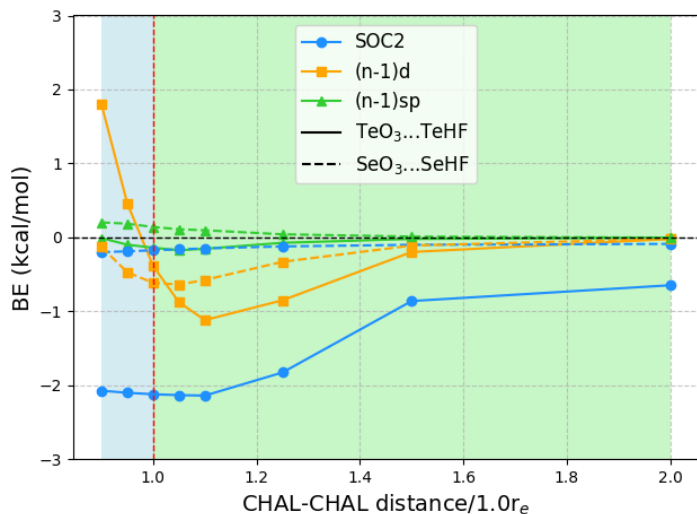


Fig. 1 Impact of Second-Order Spin-Orbit Coupling (SOC2) on the binding energies of 24 systems calculated at the CAM-B3LYP/aug-cc-pVQZ-DK Level, accompanied by subvalence (n-1)d and (n-1)sp correlation contributions determined at the cPNO-LCCSD(T) half-CP Level. Positive BE values signify dimer stabilization.)

to destabilization, but now the inner-shell subvalence (n-1)d begins to stabilize the  $\text{TeO}_3 \cdots \text{TeHF}$  dimer, resulting in opposing corrective effects. Conversely, upon stretching the  $\text{TeO}_3 \cdots \text{TeHF}$ , SOC2 remains constant up to a distance of  $1.10r_e$ , but the subvalence (n-1)d destabilizes by  $-1.117$  kcal/mol. As the Te-Te distance is further extended, both effects aim to diminish. At a distance of  $2.0r_e$ , the (n-1)d effects become negligible, although the contribution of SOC2 remains significant at  $-0.6$  kcal/mol.

For the Se complexes, SOC2 effects are still noticeable but much less significant, consistent with the apparent<sup>44</sup>  $\propto Z^4$  proportionality of SOC2. (By way of illustration: already in 1998, Runeberg and Pyykkö<sup>88</sup> found that the SOC2 stabilizations of  $\text{Xe}_2$  and  $\text{Rn}_2$  are 0.7 and 4.5 meV, respectively — a ratio of  $6.4 \approx (86/54)^4$ . Similarly, Feller et al.<sup>42</sup> found SOC2 stabilizations of 0.4 and 2.0 kcal/mol, respectively, for  $\text{Br}_2$  and  $\text{I}_2$  diatomics, consistent with  $(53/35)^4 \approx 5.3$ .) For example, at equilibrium distances, subvalence (n-1)d and SOC2 destabilize the dimer by  $-0.614$  and  $-0.173$  kcal/mol, respectively. When we compress the Se-Se distances, SOC2 remains constant, but the contribution from (n-1)d decreases, albeit still maintaining a destabilizing effect. As we extend the Se-Se distances, both SOC2 and subvalence (n-1)d contributions converge to zero. Once again, the effect of subvalence (n-1)sp remains negligible throughout.

For  $\text{SO}_3 \cdots \text{SHF}$ , the impacts of both subvalence (n-1)sp and SOC2 remain negligible, as presented in the SI.

### 3.4 Nature of non-covalent chalcogen interactions

Finally, we investigate the nature of non-covalent interactions present in all 24 systems considered in this manuscript. Symmetry-Adapted Perturbation Theory (SAPT, see Ref.<sup>81</sup> for a review) provides a systematic framework for breaking down the total interaction energy into distinct components, thus clarifying the nature of intermolecular forces. Following the notation

of Refs.<sup>62,82</sup>, at the two least expensive levels of SAPT, namely SAPT0 and SAPT2, the interaction energy can be partitioned as follows:

$$IE_{SAPT0} = E_{elst}^{(10)} + E_{exch}^{(10)} + E_{ind}^{(20)} + E_{exch-ind}^{(20)} + E_{disp}^{(20)} + E_{exch-disp}^{(20)} \quad (1)$$

$$IE_{SAPT2} = IE_{SAPT0} + E_{elst}^{(12)} + E_{exch-elst}^{(12)} + E_{ind}^{(22)} + E_{exch-ind}^{(22)} \quad (2)$$

where the terms colored in blue denote attractive forces, those in red represent repulsive forces, while terms in black may exhibit either attractive or repulsive behavior. The two superscripts indicate the order of intermolecular and intramolecular perturbation theory, respectively, while the subscripts "exch", "elst", and "ind", and correspond to exchange repulsion, electrostatic interaction, and induction, respectively. Our SAPT findings, calculated using the def2-QZVPP basis set, are documented in the Supporting Information.

Before delving into our results, let us consider various indices that have been developed to identify the nature of non-covalent interactions. The Hobza Dispersion/Electrostatic ratio<sup>89</sup> uses the information from the above equations:  $D/E \geq 1.7$  is deemed dispersion-dominant,  $D/E \leq 0.59$  (i.e.,  $1/1.7$ ) electrostatic-dominant, and the range in between 'mixed-influence'.

One of us has proposed alternative indices (see Ref. 62) that only entail MP2 calculations and do not necessitate SAPT computations. The first of these approaches is the correlation spin polarization index (CSPI), which serves as an indicator of the nature of non-covalent interactions.

$$CSPI = \frac{IE_{ss}^{(2)} - IE_{ab}^{(2)}}{IE_{ss}^{(2)} + IE_{ab}^{(2)}} \quad (3)$$

In systems where the interaction energy is primarily governed by dispersion forces, CSPI tends to approach zero. However, in systems where non-dispersion factors contribute to the correlation portion of the interaction energy, CSPI will deviate significantly from zero.

Nevertheless, in the case of nearly dissociated dimers, the absolute values of  $IE_{aa}$  and  $IE_{ab}$  become so small that the CSPI may change sign. To address this issue, the authors have also introduced the DEBC index (dispersion-electrostatic balance in correlation).

$$DEBC = \sqrt{\frac{CSPI^2}{1 + CSPI^2}} \quad (4)$$

DEBC spans a scale from 0, indicating a system dominated purely by dispersive forces, to 1, indicating a system governed solely by non-dispersive interactions. This should be considered in tandem with %HF (Percentage of Hartree-Fock in the interaction energy), which is defined as follows:

$$\%HF = \frac{(100\%)IE_{SCF}}{IE_{SCF} + IE_{aa}^{(2)} + IE_{bb}^{(2)}} \quad (5)$$

The %HF value tend towards 100% in systems where binding primarily results from pure electrostatic effects such as dipole-dipole interactions.

Returning now to the 24 chalcogen bonded systems investi-

gated in this paper, Table 4 displays the NDF2, CSPI, DEBC, Hobza ratio (dispersion/ electrostatic), and %HF for all 24 chalcogen bonded dimers. Additionally, interaction energies computed using cPNO-LCCSD(T) are included in the last column.

At equilibrium distances, the Hobza ratios for the  $TeO_3 \cdots TeHF$ ,  $SeO_3 \cdots SeHF$ , and  $SO_3 \cdots SHF$  complexes are 0.40, 0.33, and 0.34, respectively. These values suggest that the interactions lean towards the electrostatic-dominated end of the spectrum, albeit to a lesser extent than a purely hydrogen-bonded complex like the acetic acid dimer, for which the value is around 0.5, as reported in Table 16 of the Ref. 62. %HF also indicates that Te complexes are dominated by electrostatic effects, followed by Se and S, a trend consistent with CSPI and DEBC analyses.

Moreover, in all three complexes, even the stretched geometries persist within the electrostatic realm (more towards the 'mixed-influence') as indicated by the Hobza ratios of 0.57, 0.72, 0.62, respectively, for the Te, Se and S complexes. The respective %HF values are 93%, 79%, and 76% respectively.

Therefore, although definitive conclusions regarding the nature of NCIs investigated in this study are challenging to draw, it is evident that dispersion effects are minimal across all 24 complexes examined.

## 4 Conclusions

Our computational investigation into chalcogen bonding interactions has led us to conclude the following:

1. The inclusion of inner-shell  $(n-1)d$  subvalence correlation destabilizes chalcogen dimers by nontrivial amounts—a trend opposite to that observed for halogen bonding interactions in Ref. 37. (At highly compressed geometries, however, subvalence d correlation begins to stabilize the complex.) Among the various interaction energies components computed at the PNO-LCCSD(T) or DF-CCSD levels, the PNO-LMP2 or DF-MP2 component of the  $(n-1)d$  correlation constitutes the lion's share, which could prove useful in future investigations. Keeping the  $(n-1)d$  correlation treatment down to the MP2 level affords significant savings in CPU time and memory/storage overhead.
2. The effect of the lower  $(n-1)sp$  subvalence correlation is notably less pronounced. The PNO-LMP2 and (T) components exert opposing influences, leading to error cancellation at the cPNO-LCCSD(T) level. Therefore, if one is limited to MP2 level calculations, it is essential to also include  $(n-1)sp$  subvalence correlation.
3. For the Te complexes, the effects of second-order spin-orbit coupling (SOC2) rival those of  $(n-1)d$  correlation. For the Se complexes, SOC2 effects are still noticeable but much less significant, consistent with the approximate  $\propto Z^4$  proportionality of SOC2. SOC2 stabilizes the monomer more than the dimer (as the dimer orbitals are separated further and hence the denominator in the interaction is reduced), and as a result destabilizes the dimers. At equilibrium and stretched geometries, SOC2 and  $(n-1)d$  destabilize the complex in tandem; at compressed geometries, however, they

work in opposite directions as  $(n-1)d$  becomes stabilizing there.

4. We observe that all three complexes,  $\text{TeO}_3 \cdots \text{TeHF}$ ,  $\text{SeO}_3 \cdots \text{SeHF}$ , and  $\text{SO}_3 \cdots \text{SHF}$ , tend towards the electrostatic-dominated end of the spectrum at shorter, but enter a mixed-influence regime at longer, intermonomer separations.
5. Employing complete basis set (CBS) extrapolation along with CP correction appears to be the most effective strategy. Interestingly, {T,Q}Z extrapolation outperforms the 5Z basis set, highlighting its potential superiority in these analyses. Additionally, we observe a slower-than-usual convergence of basis sets for the SCF component.

Table 1 RMS Deviations (kcal/mol) for different components of total interaction energies computed across different basis sets utilizing localized and canonical approaches. The statistics pertain to 'valence + subvalence(n-1)d' electron correlation. Corresponding tables for 'Valence only' and 'Valence + (n-1)spd' are provided in the Supporting Information

		raw				halfCP				fullCP			
		Te	Se	S	All	Te	Se	S	All	Te	Se	S	All
TZ Normal	HF	0.280	0.224	1.082	0.658	0.420	0.065	0.533	0.393	0.565	0.233	0.550	0.475
	PNO-LMP2	1.800	1.142	0.794	1.314	2.597	1.664	1.224	1.916	3.402	2.194	1.660	2.526
	PNO-LCCSD	1.912	1.178	0.853	1.387	2.615	1.655	1.246	1.926	3.322	2.136	1.641	2.469
	(T)	0.270	0.246	0.180	0.235	0.342	0.293	0.212	0.287	0.416	0.340	0.245	0.341
	PNO-LCCSD(T)	2.165	1.418	1.030	1.608	2.944	1.943	1.456	2.203	3.727	2.472	1.884	2.802
QZ Normal	CCSD-MP2	0.167	0.131	0.105	0.137	0.099	0.107	0.067	0.093	0.113	0.108	0.048	0.094
	CCSD(T)-MP2	0.388	0.300	0.250	0.318	0.364	0.292	0.238	0.302	0.340	0.285	0.227	0.288
	HF	0.017	0.052	0.133	0.083	0.046	0.015	0.123	0.076	0.079	0.024	0.114	0.081
	PNO-LMP2	0.866	0.639	0.466	0.677	1.268	0.871	0.661	0.967	1.677	1.117	0.862	1.265
	PNO-LCCSD	0.850	0.589	0.475	0.657	1.143	0.777	0.616	0.874	1.440	0.969	0.760	1.094
5Z Normal	(T)	0.182	0.184	0.118	0.164	0.207	0.195	0.123	0.179	0.231	0.206	0.128	0.193
	PNO-LCCSD(T)	1.023	0.771	0.592	0.815	1.341	0.969	0.739	1.046	1.662	1.173	0.887	1.281
	CCSD-MP2	0.072	0.108	0.073	0.086	0.133	0.121	0.066	0.110	0.240	0.159	0.108	0.177
	CCSD(T)-MP2	0.185	0.172	0.148	0.169	0.109	0.122	0.091	0.108	0.081	0.073	0.038	0.067
	HF	0.012	0.011	0.049	0.030	0.016	0.005	0.043	0.026	0.020	0.002	0.036	0.024
TQZ Normal	PNO-LMP2	0.513	0.406	0.273	0.409	0.713	0.513	0.377	0.552	0.921	0.632	0.489	0.704
	PNO-LCCSD	0.451	0.327	0.234	0.349	0.559	0.399	0.299	0.433	0.670	0.474	0.366	0.519
	(T)	0.141	0.138	0.079	0.123	0.145	0.138	0.079	0.124	0.149	0.137	0.080	0.126
	PNO-LCCSD(T)	0.585	0.463	0.312	0.467	0.697	0.535	0.378	0.552	0.811	0.610	0.446	0.640
	CCSD-MP2	0.084	0.108	0.062	0.087	0.158	0.127	0.085	0.127	0.253	0.163	0.126	0.188
Q5Z Normal	CCSD(T)-MP2	0.113	0.114	0.074	0.102	0.072	0.067	0.040	0.061	0.130	0.043	0.052	0.085
	HF	0.097	0.025	0.632	0.369	0.111	0.030	0.372	0.225	0.125	0.064	0.228	0.155
	PNO-LMP2	0.138	0.260	0.191	0.203	0.121	0.206	0.158	0.165	0.131	0.161	0.135	0.143
	PNO-LCCSD	0.153	0.208	0.216	0.195	0.151	0.181	0.178	0.170	0.150	0.160	0.143	0.152
	(T)	0.119	0.139	0.073	0.114	0.109	0.124	0.058	0.101	0.100	0.109	0.043	0.089
composite Normal	PNO-LCCSD(T)	0.258	0.337	0.289	0.296	0.251	0.300	0.236	0.264	0.245	0.268	0.187	0.236
	CCSD-MP2	0.112	0.105	0.089	0.102	0.071	0.082	0.058	0.071	0.036	0.060	0.030	0.044
	CCSD(T)-MP2	0.224	0.187	0.144	0.188	0.174	0.162	0.102	0.149	0.127	0.137	0.062	0.114
	HF	0.012	0.010	0.006	0.010	0.000	0.000	0.000	0.000	0.012	0.010	0.006	0.010
	PNO-LMP2	0.147	0.170	0.094	0.141	0.125	0.145	0.071	0.118	0.108	0.122	0.057	0.099
TZ Tight	PNO-LCCSD	0.109	0.101	0.052	0.091	0.076	0.080	0.033	0.067	0.084	0.067	0.019	0.063
	(T)	0.107	0.101	0.047	0.089	0.096	0.092	0.044	0.081	0.085	0.082	0.041	0.072
	PNO-LCCSD(T)	0.205	0.189	0.076	0.167	0.145	0.153	0.057	0.126	0.105	0.120	0.044	0.095
	CCSD-MP2	0.062	0.084	0.045	0.066	0.058	0.072	0.044	0.059	0.070	0.063	0.048	0.061
	CCSD(T)-MP2	0.127	0.117	0.056	0.105	0.089	0.094	0.042	0.079	0.062	0.072	0.033	0.058
QZ Tight	HF	0.012	0.010	0.006	0.010	0.000	0.000	0.000	0.000	0.012	0.010	0.006	0.010
	PNO-LMP2	0.074	0.049	0.043	0.057	0.058	0.051	0.032	0.048	0.051	0.058	0.039	0.050
	PNO-LCCSD	0.059	0.026	0.032	0.042	0.028	0.041	0.028	0.033	0.072	0.069	0.030	0.060
	(T)	0.084	0.061	0.030	0.062	0.072	0.053	0.029	0.054	0.060	0.045	0.029	0.047
	PNO-LCCSD(T)	0.140	0.070	0.031	0.092	0.074	0.044	0.022	0.051	0.047	0.048	0.018	0.040
5Z Tight	CCSD-MP2	0.044	0.052	0.017	0.041	0.046	0.062	0.033	0.049	0.068	0.077	0.058	0.068
	CCSD(T)-MP2	0.096	0.057	0.033	0.067	0.056	0.042	0.019	0.042	0.039	0.044	0.033	0.039
	HF	0.280	0.224	1.082	0.658	0.420	0.065	0.533	0.393	0.565	0.233	0.550	0.475
	PNO-LMP2	1.734	1.014	0.685	1.225	2.548	1.565	1.142	1.848	3.368	2.122	1.607	2.478
	PNO-LCCSD	1.850	1.038	0.758	1.301	2.544	1.516	1.158	1.836	3.242	2.001	1.565	2.378
TQZ Tight	(T)	0.176	0.137	0.112	0.144	0.258	0.192	0.152	0.205	0.339	0.246	0.192	0.266
	PNO-LCCSD(T)	2.017	1.170	0.866	1.436	2.794	1.704	1.308	2.035	3.575	2.244	1.755	2.639
	CCSD-MP2	0.122	0.030	0.076	0.085	0.029	0.054	0.019	0.037	0.129	0.124	0.044	0.106
	CCSD(T)-MP2	0.297	0.159	0.187	0.222	0.258	0.142	0.168	0.196	0.221	0.126	0.150	0.170
	HF	0.017	0.052	0.133	0.083	0.046	0.015	0.123	0.076	0.079	0.024	0.114	0.081
Q5Z Tight	PNO-LMP2	0.809	0.506	0.371	0.591	1.228	0.780	0.599	0.908	1.649	1.056	0.829	1.228
	PNO-LCCSD	0.799	0.453	0.407	0.580	1.092	0.645	0.554	0.799	1.386	0.841	0.702	1.020
	(T)	0.116	0.091	0.069	0.094	0.144	0.108	0.080	0.114	0.171	0.124	0.092	0.133
	PNO-LCCSD(T)	0.908	0.540	0.474	0.669	1.230	0.750	0.633	0.909	1.552	0.963	0.793	1.150
	CCSD-MP2	0.030	0.057	0.039	0.044	0.138	0.137	0.046	0.115	0.264	0.217	0.129	0.211
composite Tight	CCSD(T)-MP2	0.117	0.038	0.107	0.094	0.053	0.034	0.037	0.042	0.109	0.095	0.038	0.086
	HF	0.012	0.011	0.049	0.030	0.016	0.005	0.043	0.026	0.020	0.002	0.036	0.024
	PNO-LMP2	0.455	0.282	0.192	0.328	0.674	0.426	0.328	0.498	0.893	0.572	0.465	0.669
	PNO-LCCSD	0.411	0.229	0.196	0.294	0.525	0.304	0.267	0.383	0.639	0.379	0.339	0.471
	(T)	0.080	0.063	0.044	0.064	0.086	0.067	0.049	0.069	0.093	0.071	0.053	0.074
TZ Normal	PNO-LCCSD(T)	0.486	0.290	0.239	0.355	0.606	0.369	0.315	0.448	0.727	0.449	0.391	0.543
	CCSD-MP2	0.047	0.055	0.009	0.042	0.150	0.124	0.061	0.118	0.255	0.194	0.127	0.199
	CCSD(T)-MP2	0.051	0.013	0.051	0.042	0.075	0.059	0.014	0.056	0.169	0.124	0.074	0.128
	HF	0.097	0.025	0.632	0.369	0.111	0.030	0.372	0.225	0.125	0.064	0.228	0.155
	PNO-LMP2	0.046	0.042	0.091	0.064	0.040	0.063	0.103	0.073	0.088	0.085	0.118	0.098
QZ Normal	PNO-LCCSD	0.064	0.050	0.165	0.106	0.075	0.047	0.131	0.092	0.088	0.046	0.099	0.081
	(T)	0.072	0.057	0.038	0.058	0.061	0.046	0.029	0.047	0.051	0.036	0.020	0.038
	PNO-LCCSD(T)	0.134	0.098	0.203	0.151	0.134	0.084	0.159	0.130	0.134	0.072	0.118	0.111
	CCSD-MP2	0.105	0.025	0.078	0.077	0.064	0.037	0.032	0.046	0.036	0.059	0.028	0.043
	CCSD(T)-MP2	0.173	0.059	0.114	0.124	0.118	0.030	0.057	0.078	0.067	0.031	0.018	0.044
5Z Normal	HF	0.012	0.010	0.006	0.010	0.000	0.000	0.000	0.000	0.012	0.010	0.006	0.010
	PNO-LMP2	0.031	0.017	0.026	0.025	0.005	0.001	0.001	0.003	0.022	0.019	0.026	0.023
	PNO-LCCSD	0.052	0.022	0.006	0.033	0.007	0.018	0.005	0.011	0.058	0.054	0.010	0.046
	(T)	0.050	0.040	0.025	0.040	0.041	0.034	0.023	0.033	0.033	0.027	0.021	0.028
	PNO-LCCSD(T)	0.101	0.062	0.026	0.070	0.037	0.021	0.024	0.028	0.032	0.030	0.024	0.029
TQZ Normal	CCSD-MP2	0.022	0.014	0.025	0.021	0.010	0.017	0.004	0.012	0.038	0.038	0.025	0.034
	CCSD(T)-MP2	0.071	0.049	0.049	0.057	0.033	0.021	0.023	0.026	0.020	0.015	0.008	0.015
	HF	0.012	0.010	0.006	0.010					0.012	0.010	0.006	0.010
	PNO-LMP2	0.024	0.017	0.027	0.023					0.024	0.017	0.027	0.023

TZ	HF	0.280	0.224	1.082	0.658	0.420	0.065	0.533	0.393	0.565	0.233	0.550	0.475
	PNO-LMP2	1.713	0.998	0.673	1.209	2.529	1.551	1.131	1.833	3.351	2.111	1.597	2.465
vTight	PNO-LCCSD	1.827	1.013	0.743	1.280	2.518	1.488	1.140	1.813	3.214	1.971	1.544	2.352
	(T)	0.125	0.084	0.064	0.094	0.209	0.139	0.103	0.156	0.293	0.194	0.142	0.219
	PNO-LCCSD(T)	1.949	1.095	0.806	1.372	2.725	1.625	1.242	1.967	3.506	2.163	1.685	2.569
	CCSD-MP2	0.118	0.031	0.072	0.082	0.027	0.073	0.014	0.046	0.140	0.146	0.055	0.121
QZ	CCSD(T)-MP2	0.242	0.098	0.135	0.170	0.201	0.077	0.112	0.140	0.161	0.057	0.089	0.111
	HF	0.017	0.052	0.133	0.083	0.046	0.015	0.123	0.076	0.079	0.024	0.114	0.081
vTight	PNO-LMP2	0.791	0.497	0.363	0.579	1.213	0.773	0.593	0.899	1.638	1.053	0.826	1.221
	PNO-LCCSD	0.793	0.458	0.399	0.577	1.084	0.650	0.546	0.795	1.377	0.844	0.694	1.015
	(T)	0.049	0.029	0.020	0.035	0.079	0.047	0.033	0.056	0.110	0.065	0.046	0.078
	PNO-LCCSD(T)	0.841	0.486	0.419	0.611	1.162	0.696	0.579	0.851	1.486	0.909	0.739	1.092
	CCSD-MP2	0.028	0.041	0.038	0.036	0.131	0.125	0.049	0.108	0.263	0.210	0.133	0.209
	CCSD(T)-MP2	0.061	0.015	0.059	0.050	0.061	0.079	0.019	0.059	0.157	0.145	0.088	0.133
TQZ	HF	0.097	0.025	0.632	0.369	0.111	0.030	0.372	0.225	0.125	0.064	0.228	0.155
	PNO-LMP2	0.058	0.040	0.088	0.065	0.034	0.063	0.103	0.073	0.082	0.088	0.121	0.098
vTight	PNO-LCCSD	0.072	0.071	0.163	0.111	0.082	0.064	0.130	0.096	0.091	0.058	0.099	0.085
	(T)	0.017	0.013	0.012	0.014	0.023	0.021	0.018	0.021	0.030	0.029	0.024	0.028
	PNO-LCCSD(T)	0.064	0.060	0.153	0.102	0.066	0.048	0.113	0.080	0.068	0.038	0.076	0.063
	CCSD-MP2	0.125	0.033	0.078	0.087	0.076	0.008	0.030	0.048	0.038	0.031	0.026	0.032
Canonical	CCSD(T)-MP2	0.118	0.023	0.067	0.079	0.064	0.022	0.017	0.040	0.039	0.059	0.050	0.050
	DF-MP2	1.688	0.975	0.654	1.187	2.504	1.527	1.110	1.810	3.327	2.090	1.578	2.445
TZ	DF-CCSD	1.787	0.967	0.707	1.242	2.476	1.438	1.100	1.771	3.173	1.920	1.504	2.311
	CCSD-MP2	0.107	0.061	0.058	0.079	0.061	0.114	0.033	0.077	0.168	0.185	0.082	0.152
QZ	DF-MP2	0.765	0.473	0.341	0.555	1.186	0.749	0.571	0.875	1.613	1.032	0.806	1.199
	DF-CCSD	0.783	0.439	0.390	0.565	1.069	0.627	0.536	0.780	1.359	0.820	0.684	0.998
	CCSD-MP2	0.035	0.056	0.054	0.049	0.124	0.135	0.044	0.109	0.258	0.220	0.127	0.209
	DF-MP2	0.093	0.032	0.058	0.066	0.045	0.045	0.079	0.059	0.060	0.068	0.100	0.078
TQZ	DF-CCSD	0.092	0.082	0.171	0.122	0.096	0.076	0.141	0.108	0.101	0.070	0.113	0.096
	CCSD-MP2	0.161	0.063	0.115	0.120	0.106	0.041	0.066	0.076	0.056	0.043	0.030	0.044

Table 2 RMS Deviations (kcal/mol) of the subvalence (n−1)d component for different components of the total interaction energies computed across different basis sets utilizing localized and canonical approaches. Corresponding table for subvalence '(n−1)sp' component is provided in the Supporting Information.

		raw		half-CP		full-CP	
		Te	Se	Te	Se	Te	Se
TZ	PNO-LMP2	0.268	0.097	0.376	0.062	0.530	0.091
	PNO-LCCSD	0.237	0.140	0.276	0.088	0.396	0.073
	(T)	0.026	0.011	0.040	0.014	0.055	0.018
	PNO-LCCSD(T)	0.249	0.134	0.309	0.085	0.449	0.084
	CCSD-MP2	0.132	0.048	0.143	0.050	0.154	0.053
QZ	CCSD(T)-MP2	0.111	0.041	0.108	0.040	0.104	0.038
	PNO-LMP2	0.120	0.035	0.157	0.028	0.233	0.046
	PNO-LCCSD	0.106	0.051	0.123	0.034	0.188	0.042
	(T)	0.028	0.018	0.034	0.019	0.040	0.019
	PNO-LCCSD(T)	0.105	0.039	0.145	0.036	0.224	0.056
5Z	CCSD-MP2	0.040	0.020	0.045	0.016	0.050	0.013
	CCSD(T)-MP2	0.026	0.013	0.025	0.012	0.025	0.012
	PNO-LMP2	0.067	0.018	0.086	0.015	0.118	0.024
	PNO-LCCSD	0.053	0.025	0.062	0.021	0.087	0.027
	(T)	0.032	0.021	0.033	0.020	0.033	0.019
TQZ	PNO-LCCSD(T)	0.056	0.021	0.081	0.029	0.112	0.041
	CCSD-MP2	0.029	0.011	0.033	0.010	0.038	0.008
	CCSD(T)-MP2	0.029	0.019	0.026	0.019	0.025	0.018
	PNO-LMP2	0.077	0.030	0.059	0.016	0.042	0.005
	PNO-LCCSD	0.024	0.020	0.018	0.024	0.049	0.031
Q5Z	(T)	0.033	0.024	0.033	0.023	0.032	0.021
	PNO-LCCSD(T)	0.018	0.043	0.047	0.046	0.079	0.050
	CCSD-MP2	0.059	0.019	0.075	0.016	0.091	0.026
	CCSD(T)-MP2	0.089	0.024	0.105	0.034	0.121	0.046
	PNO-LMP2	0.028	0.004	0.003	0.001	0.027	0.005
Normal	PNO-LCCSD	0.024	0.013	0.017	0.013	0.025	0.014
	(T)	0.037	0.023	0.032	0.021	0.028	0.019
	PNO-LCCSD(T)	0.056	0.032	0.035	0.030	0.019	0.027
	CCSD-MP2	0.016	0.011	0.014	0.013	0.018	0.015
	CCSD(T)-MP2	0.029	0.028	0.034	0.029	0.039	0.031
composite	PNO-LMP2	0.029	0.009	0.007	0.005	0.027	0.004
	PNO-LCCSD	0.026	0.013	0.017	0.011	0.025	0.009
	(T)	0.024	0.012	0.019	0.010	0.015	0.008
	PNO-LCCSD(T)	0.044	0.020	0.023	0.015	0.015	0.011
	CCSD-MP2	0.013	0.005	0.010	0.007	0.014	0.009
TZ	CCSD(T)-MP2	0.016	0.014	0.019	0.014	0.023	0.014
	PNO-LMP2	0.280	0.109	0.380	0.069	0.530	0.092
	PNO-LCCSD	0.231	0.157	0.259	0.102	0.372	0.069
	(T)	0.026	0.016	0.026	0.012	0.034	0.009
	PNO-LCCSD(T)	0.257	0.173	0.284	0.114	0.405	0.077
QZ	CCSD-MP2	0.136	0.057	0.153	0.065	0.171	0.072
	CCSD(T)-MP2	0.140	0.072	0.142	0.075	0.144	0.078
	PNO-LMP2	0.129	0.045	0.160	0.033	0.233	0.046
	PNO-LCCSD	0.111	0.062	0.119	0.040	0.177	0.031
	(T)	0.010	0.006	0.013	0.005	0.017	0.004
Tight	PNO-LCCSD(T)	0.121	0.067	0.132	0.044	0.194	0.034
	CCSD-MP2	0.038	0.023	0.047	0.025	0.057	0.028

5Z	CCSD(T)-MP2	0.032	0.028	0.037	0.029	0.041	0.031
	PNO-LMP2	0.071	0.023	0.088	0.018	0.118	0.024
	PNO-LCCSD	0.053	0.030	0.058	0.020	0.079	0.015
Tight	(T)	0.006	0.002	0.007	0.002	0.008	0.002
	PNO-LCCSD(T)	0.057	0.031	0.064	0.022	0.087	0.017
	CCSD-MP2	0.026	0.011	0.033	0.013	0.040	0.016
TQZ	CCSD(T)-MP2	0.021	0.011	0.026	0.014	0.032	0.017
	PNO-LMP2	0.077	0.019	0.059	0.012	0.042	0.005
	PNO-LCCSD	0.032	0.010	0.022	0.012	0.044	0.015
Tight	(T)	0.008	0.003	0.007	0.001	0.006	0.001
	PNO-LCCSD(T)	0.028	0.013	0.026	0.013	0.050	0.014
	CCSD-MP2	0.060	0.012	0.073	0.005	0.086	0.010
Q5Z	CCSD(T)-MP2	0.068	0.010	0.079	0.005	0.092	0.010
	PNO-LMP2	0.028	0.005	0.001	0.000	0.026	0.004
	PNO-LCCSD	0.016	0.002	0.003	0.002	0.019	0.003
Tight	(T)	0.007	0.002	0.004	0.001	0.002	0.000
	PNO-LCCSD(T)	0.023	0.004	0.003	0.002	0.018	0.003
	CCSD-MP2	0.013	0.004	0.004	0.002	0.008	0.002
composite	CCSD(T)-MP2	0.006	0.003	0.003	0.002	0.009	0.002
	PNO-LMP2	0.027	0.004	REF		0.027	0.004
	PNO-LCCSD	0.017	0.003			0.017	0.003
Tight	(T)	0.003	0.001			0.003	0.001
	PNO-LCCSD(T)	0.020	0.003			0.020	0.003
	CCSD-MP2	0.010	0.003			0.010	0.003
TZ	CCSD(T)-MP2	0.007	0.002			0.007	0.002
	PNO-LMP2	0.279	0.109	0.379	0.069	0.529	0.092
	PNO-LCCSD	0.241	0.156	0.260	0.099	0.368	0.069
vTight	(T)	0.030	0.018	0.026	0.014	0.032	0.010
	PNO-LCCSD(T)	0.269	0.174	0.285	0.113	0.399	0.076
	CCSD-MP2	0.141	0.056	0.159	0.061	0.177	0.067
QZ	CCSD(T)-MP2	0.152	0.073	0.154	0.074	0.156	0.074
	PNO-LMP2	0.129	0.045	0.159	0.033	0.232	0.046
	PNO-LCCSD	0.111	0.060	0.118	0.037	0.176	0.030
vTight	(T)	0.014	0.008	0.012	0.007	0.014	0.005
	PNO-LCCSD(T)	0.125	0.068	0.129	0.043	0.189	0.032
	CCSD-MP2	0.038	0.021	0.047	0.023	0.057	0.025
TQZ	CCSD(T)-MP2	0.039	0.028	0.043	0.029	0.048	0.029
	PNO-LMP2	0.080	0.019	0.061	0.011	0.044	0.005
	PNO-LCCSD	0.024	0.012	0.020	0.014	0.046	0.016
vTight	(T)	0.002	0.001	0.003	0.002	0.004	0.003
	PNO-LCCSD(T)	0.026	0.011	0.020	0.012	0.044	0.013
	CCSD-MP2	0.065	0.009	0.077	0.004	0.090	0.011
Canonical	CCSD(T)-MP2	0.064	0.010	0.076	0.003	0.087	0.009
	DF-MP2	0.283	0.111	0.380	0.070	0.529	0.092
	DF-CCSD	0.244	0.153	0.260	0.094	0.368	0.058
QZ	CCSD-MP2	0.145	0.058	0.161	0.065	0.177	0.071
	DF-MP2	0.132	0.047	0.160	0.033	0.232	0.046
	DF-CCSD	0.108	0.053	0.117	0.030	0.177	0.026
TQZ	CCSD-MP2	0.040	0.022	0.048	0.024	0.057	0.026
	DF-MP2	0.080	0.018	0.062	0.011	0.044	0.005
	DF-CCSD	0.018	0.022	0.027	0.023	0.054	0.025
	CCSD-MP2	0.074	0.011	0.086	0.015	0.097	0.022

Table 3 The (n–1)d component of total interaction energies (in kcal/mol), computed at the composite PNO-LCCSD(T) and CCSD/hAWCV{T,Q}Z levels. It includes breakdowns of the (n–1)d contributions into MP2, CCSD, (T), and CCSD-MP2. Heatmapping is employed to illustrate the contribution's impact on dimer stability, ranging from blue (stabilizing) to red (destabilizing). Additionally, the lower panel of the table presents RMSD and MAD values (in kcal/mol). Here, the heat mapping indicates deviations, ranging from red (for larger deviations) transitioning to yellow and green (for smaller deviations).

	PNO-LMP2	PNO-LCCSD	(T)	PNO-LCCSD(T)	CCSD-MP2	CCSD(T)-MP2	MP2	CCSD	CCSD-MP2
<b>TeO<sub>3</sub>...TeHF</b>									
0.9r <sub>e</sub>	2.553	1.774	0.027	1.802	-0.778	-0.751	2.662	1.721	-0.941
0.95r <sub>e</sub>	0.665	0.426	0.035	0.461	-0.240	-0.205	0.750	0.392	-0.357
1.0r <sub>e</sub>	-0.463	-0.426	0.040	-0.386	0.037	0.077	-0.394	-0.444	-0.050
1.05r <sub>e</sub>	-1.025	-0.901	0.025	-0.876	0.124	0.149	-0.967	-0.912	0.055
1.10r <sub>e</sub>	-1.196	-1.099	-0.018	-1.117	0.097	0.080	-1.147	-1.102	0.045
1.25r <sub>e</sub>	-0.774	-0.761	-0.088	-0.849	0.013	-0.076	-0.745	-0.776	-0.031
1.50r <sub>e</sub>	-0.219	-0.174	-0.022	-0.196	0.044	0.022	-0.214	-0.200	0.014
2.0r <sub>e</sub>	-0.059	-0.017	-0.003	-0.021	0.042	0.038	-0.058	-0.036	0.021
<b>SeO<sub>3</sub>...SeHF</b>									
0.9r <sub>e</sub>	0.012	-0.141	0.012	-0.129	-0.153	-0.141	-0.006	-0.178	-0.173
0.95r <sub>e</sub>	-0.385	-0.463	-0.006	-0.469	-0.078	-0.085	-0.403	-0.488	-0.085
1.0r <sub>e</sub>	-0.537	-0.590	-0.025	-0.614	-0.053	-0.077	-0.551	-0.607	-0.056
1.05r <sub>e</sub>	-0.554	-0.596	-0.041	-0.636	-0.042	-0.083	-0.564	-0.611	-0.048
1.10r <sub>e</sub>	-0.507	-0.528	-0.045	-0.574	-0.022	-0.067	-0.513	-0.555	-0.042
1.25r <sub>e</sub>	-0.298	-0.295	-0.034	-0.329	0.003	-0.031	-0.300	-0.320	-0.020
1.50r <sub>e</sub>	-0.114	-0.098	-0.010	-0.109	0.015	0.005	-0.116	-0.116	0.000
2.0r <sub>e</sub>	-0.028	-0.014	-0.004	-0.017	0.014	0.011	-0.026	-0.022	0.005
	Te	Se		Te	Se		RMSD		MAD
PNO-LMP2	1.135	0.371		0.869	0.304		DF-MP2	1.154	0.379 0.867 0.310
PNO-LCCSD	0.876	0.405		0.697	0.341		DF-CCSD	0.866	0.424 0.698 0.362
(T)	0.040	0.027		0.032	0.022				
PNO-LCCSD(T)	0.893	0.428		0.713	0.360				
CCSD-MP2	0.294	0.066		0.172	0.048		CCSD-MP2	0.358	0.075 0.189 0.054
CCSD(T)-MP2	0.285	0.075		0.175	0.062				

Table 4 Indices delineating noncovalent interaction types and their progression along the dissociation curve for all 24 chalcogen-bonded complexes investigated in this study. Computed interaction energies (kcal/mol) at DF-CCSD/hAWCV{T,Q} and cPNO-LCCSD(T) levels are included for clarity.

	CSPI	DEBC	Hobza ratio	%HF	DF-CCSD/{T,Q}Z BE (kcal/mol)	cPNO-LCCSD(T) BE (kcal/mol)
<b>TeO<sub>3</sub>...TeHF</b>						
0.90r <sub>e</sub>	-88.398	1.000	0.38	100.51	23.221	21.191
0.95r <sub>e</sub>	8.424	0.993	0.39	96.55	30.523	29.398
1.0r <sub>e</sub>	3.146	0.953	0.40	92.59	31.278	30.980
1.05r <sub>e</sub>	1.837	0.878	0.42	88.74	28.525	28.837
1.10r <sub>e</sub>	1.355	0.805	0.44	85.41	24.285	24.898
1.25r <sub>e</sub>	1.098	0.739	0.51	80.05	12.701	12.976
1.50r <sub>e</sub>	1.037	0.720	0.64	80.86	5.137	5.297
2.0r <sub>e</sub>	1.910	0.886	0.57	93.16	1.282	1.331
<b>SeO<sub>3</sub>...SeHF</b>						
0.90r <sub>e</sub>	1.095	0.738	0.27	21.51	8.844	9.563
0.95r <sub>e</sub>	0.946	0.687	0.30	50.90	12.075	13.037
1.0r <sub>e</sub>	0.833	0.640	0.33	57.72	12.618	13.641
1.05r <sub>e</sub>	0.754	0.602	0.37	60.15	11.887	12.856
1.10r <sub>e</sub>	0.698	0.572	0.40	61.32	10.670	11.374
1.25r <sub>e</sub>	0.588	0.507	0.54	63.90	7.033	7.490
1.50r <sub>e</sub>	0.476	0.430	0.74	69.85	3.321	3.580
2.0r <sub>e</sub>	0.462	0.420	0.72	78.85	0.727	0.777
<b>SO<sub>3</sub>...SHF</b>						
0.90r <sub>e</sub>	0.437	0.401	0.29	-5.56	7.897	9.370
0.95r <sub>e</sub>	0.392	0.365	0.31	20.56	9.431	10.792
1.0r <sub>e</sub>	0.356	0.335	0.34	31.95	9.762	10.998
1.05r <sub>e</sub>	0.329	0.312	0.37	38.80	9.456	10.544
1.10r <sub>e</sub>	0.309	0.295	0.41	43.79	8.821	9.753
1.25r <sub>e</sub>	0.271	0.261	0.52	54.30	6.376	7.007
1.50r <sub>e</sub>	0.254	0.247	0.66	65.34	3.149	3.357
2.0r <sub>e</sub>	0.320	0.305	0.60	75.98	0.669	0.724

## Conflicts of interest

The authors declare that there is no conflict of interest.

## Acknowledgements

Work on this paper was supported by the Israel Science Foundation (grant 1969/20) and by a research grant from the Artificial Intelligence and Smart Materials Research Fund (in memory of Dr. Uriel Arnon), Israel. Nisha Mehta would like to acknowledge the Feinberg Graduate School for a Sir Charles Clore Postdoctoral Fellowship as well as Dean of the Faculty and Weizmann Postdoctoral Excellence fellowships. Nisha Mehta acknowledges the School of Chemistry, The University of Melbourne, for the Visiting Academic appointment.

## Notes and references

- 1 K. E. Riley, M. Pitoňák, P. Jurečka and P. Hobza, *Chem. Rev.*, 2010, **110**, 5023–5063.
- 2 J. Řezáč and P. Hobza, *Chem. Rev.*, 2016, **116**, 5038–5071.
- 3 K. E. Riley and P. Hobza, *Acc. Chem. Res.*, 2013, **46**, 927–936.
- 4 K. E. Riley and P. Hobza, *Wiley Interdiscip. Rev.: Comput. Mol. Sci.*, 2011, **1**, 3–17.
- 5 F. T. Burling and B. M. Goldstein, *J. Am. Chem. Soc.*, 1992, **114**, 2313–2320.
- 6 J. C. Taylor and G. D. Markham, *J. Biol. Chem.*, 1999, **274**, 32909–32914.
- 7 M. Iwaoka, S. Takemoto, M. Okada and S. Tomoda, *Chem. Lett.*, 2001, **30**, 132–133.
- 8 M. Iwaoka, S. Takemoto and S. Tomoda, *J. Am. Chem. Soc.*, 2002, **124**, 10613–10620.
- 9 M. Iwaoka, S. Takemoto, M. Okada and S. Tomoda, *Bull. Chem. Soc. Jpn.*, 2002, **75**, 1611–1625.
- 10 M. H. Coonan, I. E. Craven, M. R. Hesling, G. L. Ritchie and M. A. Spackman, *J. Phys. Chem.*, 1992, **96**, 7301–7307.
- 11 M. Iwaoka and S. Tomoda, *J. Am. Chem. Soc.*, 1996, **118**, 8077–8084.
- 12 V. I. Minkin and R. M. Minyaev, *Chem. Rev.*, 2001, **101**, 1247–1266.
- 13 P. Sanz, M. Yáñez and O. Mó, *Chem. - Eur. J.*, 2002, **8**, 3999–4007.
- 14 S. Hayashi and W. Nakanishi, *Bull. Chem. Soc. Jpn.*, 2008, **81**, 1605–1615.
- 15 G. Sánchez-Sanz, I. Alkorta and J. Elguero, *Mol. Phys.*, 2011, **109**, 2543–2552.
- 16 G. Sánchez-Sanz, C. Trujillo, I. Alkorta and J. Elguero, *ChemPhysChem*, 2012, **13**, 496–503.
- 17 M. D. Esrafil and F. Mohammadian-Sabet, *Chem. Phys. Lett.*, 2015, **628**, 71–75.
- 18 V. Bondybey and J. English, *J. Mol. Spectrosc.*, 1985, **109**, 221–228.
- 19 L. J. Larson, M. Kuno and F.-M. Tao, *J. Chem. Phys.*, 2000, **112**, 8830–8838.
- 20 T. Loerting and K. R. Liedl, *J. Phys. Chem. A*, 2001, **105**, 5137–5145.
- 21 Y. Mo and J. Gao, *J. Phys. Chem. A*, 2001, **105**, 6530–6536.
- 22 G. Merino, V. I. Bakhmutov and A. Vela, *J. Phys. Chem. A*, 2002, **106**, 8491–8494.
- 23 M. Pszozna, K. Haupa, A. Bil, K. Mierzwicki, Z. Szewczuk and Z. Mielke, *J. Mass Spectrom.*, 2015, **50**, 127–135.
- 24 L. M. Azofra, I. Alkorta and S. Scheiner, *Phys. Chem. Chem. Phys.*, 2014, **16**, 18974–18981.
- 25 L. M. Azofra, I. Alkorta and S. Scheiner, in *Noncovalent interactions in dimers and trimers of SO<sub>3</sub> and CO*, ed. M. F. Ruiz-Lopez and F. J. Olivares del Valle, Springer Berlin Heidelberg, Berlin, Heidelberg, 2016, pp. 159–166.
- 26 L. M. Azofra, I. Alkorta and S. Scheiner, *Theor. Chem. Acc.*, 2014, **133**, 1586.
- 27 L. A. Curtiss, K. Raghavachari, G. W. Trucks and J. A. Pople, *J. Chem. Phys.*, 1991, **94**, 7221–7230.
- 28 L. A. Curtiss, K. Raghavachari, P. C. Redfern and J. A. Pople, *J. Chem. Phys.*, 1997, **106**, 1063–1079.
- 29 L. A. Curtiss, K. Raghavachari, P. C. Redfern, V. Rassolov and J. A. Pople, *J. Chem. Phys.*, 1998, **109**, 7764–7776.
- 30 L. A. Curtiss, P. C. Redfern and K. Raghavachari, *J. Chem. Phys.*, 2005, **123**, 124107.
- 31 H. S. Yu, X. He, S. L. Li and D. G. Truhlar, *Chem. Sci.*, 2016, **7**, 5032–5051.
- 32 N. Mardirossian and M. Head-Gordon, *Mol. Phys.*, 2017, **115**, 2315–2372.
- 33 L. Goerigk, A. Hansen, C. Bauer, S. Ehrlich, A. Najibi and S. Grimme, *Phys. Chem. Chem. Phys.*, 2017, **19**, 32184–32215.
- 34 L. Goerigk and S. Grimme, *J. Chem. Theory Comput.*, 2010, **6**, 107–126.
- 35 L. Goerigk and S. Grimme, *J. Chem. Theory Comput.*, 2011, **7**, 291–309.
- 36 N. Mehta, T. Fellowes, J. M. White and L. Goerigk, *J. Chem. Theory Comput.*, 2021, **17**, 2783–2806.
- 37 M. K. Kesharwani, D. Manna, N. Sylvetsky and J. M. L. Martin, *J. Phys. Chem. A*, 2018, **122**, 2184–2197.
- 38 P. Schwerdtfeger, L. v. Szentpály, K. Vogel, H. Silberbach, H. Stoll and H. Preuss, *J. Chem. Phys.*, 1986, **84**, 1606–1612.
- 39 E. van Lenthe, J. G. Snijders and E. J. Baerends, *J. Chem. Phys.*, 1996, **105**, 6505–6516.
- 40 L. Visscher and K. G. Dyall, *J. Chem. Phys.*, 1996, **104**, 9040.
- 41 L. Visscher, J. Styszyński and W. C. Nieuwpoort, *J. Chem. Phys.*, 1996, **105**, 1987.
- 42 D. Feller, K. A. Peterson, W. A. de Jong and D. A. Dixon, *J. Chem. Phys.*, 2003, **118**, 3510–3522.
- 43 J.-B. Rota, S. Knecht, T. Fleig, D. Ganyushin, T. Saue, F. Neese and H. Bolvin, *J. Chem. Phys.*, 2011, **135**, 114106.
- 44 A. Karton, P. R. Taylor and J. M. L. Martin, *J. Chem. Phys.*, 2007, **127**, 064104.
- 45 M. Kurpas, P. E. Faria Junior, M. Gmitra and J. Fabian, *Phys. Rev. B*, 2019, **100**, 125422.
- 46 H.-J. Werner, P. J. Knowles, F. R. Manby, J. A. Black, K. Doll, A. Heßelmann, D. Kats, A. Köhn, T. Korona, D. A. Kreplinger et al., *J. Chem. Phys.*, 2020, **152**, 144107.
- 47 T. H. Dunning Jr, *J. Chem. Phys.*, 1989, **90**, 1007–1023.
- 48 R. A. Kendall, T. H. Dunning Jr and R. J. Harrison, *J. Chem. Phys.*, 1992, **96**, 6796–6806.
- 49 K. A. Peterson and T. H. Dunning, *J. Chem. Phys.*, 2002, **117**, 10548–10560.
- 50 D. E. Woon and T. H. Dunning, *J. Chem. Phys.*, 1993, **98**, 1358–1371.
- 51 K. A. Peterson, *J. Chem. Phys.*, 2003, **119**, 11099–11112.
- 52 K. A. Peterson, D. Figgen, E. Goll, H. Stoll and M. Dolg, *J. Chem. Phys.*, 2003, **119**, 11113–11123.
- 53 K. A. Peterson and K. E. Yousaf, *J. Chem. Phys.*, 2010, **133**, 174116.
- 54 T. Schwabe, *J. Phys. Chem. A*, 2013, **117**, 2879–2883.
- 55 G. D. Purvis and R. J. Bartlett, *J. Chem. Phys.*, 1982, **76**, 1910–1918.
- 56 K. Raghavachari, G. W. Trucks, J. A. Pople and M. Head-Gordon, *Chem. Phys. Lett.*, 1989, **157**, 479–483.
- 57 Q. Ma and H.-J. Werner, *Wiley Interdiscip. Rev. Comput. Mol. Sci.*, 2018, **8**, e1371.
- 58 See the MOLPRO online documentation at page [https://www.molpro.net/manual/doku.php?id=local\\_correlation\\_methods\\_with\\_pair\\_natural\\_orbitals\\_pnos](https://www.molpro.net/manual/doku.php?id=local_correlation_methods_with_pair_natural_orbitals_pnos).
- 59 Q. Ma and H.-J. Werner, *Journal of Chemical Theory and Computation*, 2019, **15**, 1044–1052.
- 60 J. M. L. Martin, *AIP Conf. Proc.*, 2018, **2040**, 020008.
- 61 D. W. Schwenke, *J. Chem. Phys.*, 2005, **122**, 014107.
- 62 B. Brauer, M. K. Kesharwani, S. Kozuch and J. M. L. Martin, *Phys. Chem. Chem. Phys.*, 2016, **18**, 20905–20925.
- 63 F. Neese, *Wiley Interdiscip. Rev.: Comput. Mol. Sci.*, 2012, **2**, 73–78.
- 64 F. Neese, F. Wennmohs, U. Becker and C. Riplinger, *J. Chem. Phys.*, 2020, **152**, 224108.

- 65 ORCA – an ab initio, density functional and semiempirical program package, V. 5.0.2, F. Neese, MPI für Chemische Energiekonversion, Mülheim a. d. Ruhr (Germany).
- 66 D. A. Pantazis and F. Neese, *J. Chem. Theory Comput.*, 2011, **7**, 677–684.
- 67 T. Yanai, D. P. Tew and N. C. Handy, *Chem. Phys. Lett.*, 2004, **393**, 51–57.
- 68 W. A. de Jong, R. J. Harrison and D. A. Dixon, *J. Chem. Phys.*, 2001, **114**, 48.
- 69 D. H. Bross and K. A. Peterson, *Theor. Chem. Acc.*, 2014, **133**, 1434.
- 70 F. Weigend, *Phys. Chem. Chem. Phys.*, 2006, **8**, 1057–1065.
- 71 D. A. Pantazis, X.-Y. Chen, C. R. Landis and F. Neese, *J. Chem. Theory Comput.*, 2008, **4**, 908–919.
- 72 D. A. Pantazis and F. Neese, *J. Chem. Theory Comput.*, 2009, **5**, 2229–2238.
- 73 D. A. Pantazis and F. Neese, *J. Chem. Theory Comput.*, 2011, **7**, 677–684.
- 74 D. A. Pantazis and F. Neese, *Theor. Chem. Acc.*, 2012, **131**, 1292.
- 75 C. Hättig, *Phys. Chem. Chem. Phys.*, 2005, **7**, 59–66.
- 76 A. Hellweg, C. Hättig, S. Höfener and W. Klopper, *Theor. Chem. Acc.*, 2007, **117**, 587–597.
- 77 F. Neese, *J. Chem. Phys.*, 2005, **122**, 034107.
- 78 S. F. Boys and F. Bernardi, *Mol. Phys.*, 1970, **19**, 553–566.
- 79 L. A. Burns, M. S. Marshall and C. D. Sherrill, *J. Chem. Theory Comput.*, 2014, **10**, 49–57.
- 80 B. Brauer, M. K. Kesharwani and J. M. L. Martin, *J. Chem. Theory Comput.*, 2014, **10**, 3791–3799.
- 81 K. Szalewicz, *Wiley Interdiscip. Rev.: Comput. Mol. Sci.*, 2012, **2**, 254–272.
- 82 T. M. Parker, L. A. Burns, R. M. Parrish, A. G. Ryno and C. D. Sherrill, *J. Chem. Phys.*, 2014, **140**, 094106.
- 83 D. G. A. Smith, L. A. Burns, A. C. Simmonett, R. M. Parrish, M. C. Schieber, R. Galvelis, P. Kraus, H. Kruse, R. D. Remigio, A. Alenaizan, A. M. James, S. Lehtola, J. P. Misiewicz, M. Scheurer, R. A. Shaw, J. B. Schriber, Y. Xie, Z. L. Glick, D. A. Sirianni, J. S. O'Brien, J. M. Waldrop, A. Kumar, E. G. Hohenstein, B. P. Pritchard, B. R. Brooks, H. F. Schaefer, A. Y. Sokolov, K. Patkowski, A. E. DePrince, U. Bozkaya, R. A. King, F. A. Evangelista, J. M. Turney, T. D. Crawford and C. D. Sherrill, *J. Chem. Phys.*, 2020, **152**, 184108.
- 84 A. Halkier, H. Koch, P. Jørgensen, O. Christiansen, I. M. B. Nielsen and T. Helgaker, *Theor. Chem. Acc.*, 1997, **97**, 150–157.
- 85 V. Fishman, E. Semidalas and J. M. L. Martin, *J. Phys. Chem. A*, 2024, submitted.
- 86 A. Karton, N. Sylvetsky and J. M. L. Martin, *J. Comput. Chem.*, 2017, **38**, 2063–2075.
- 87 D. S. Ranasinghe and G. A. Petersson, *J. Chem. Phys.*, 2013, **138**, 144104.
- 88 N. Runeberg and P. Pyykkö, *International Journal of Quantum Chemistry*, 1998, **66**, 131–140.
- 89 J. Řezáč, K. E. Riley and P. Hobza, *J. Chem. Theory Comput.*, 2011, **7**, 2427–2438.